Research Article

Domenico Bonaccini Calia, Wolfgang Hackenberg, Ronald Holzlöhner*, Steffan Lewis and Thomas Pfrommer

The Four-Laser Guide Star Facility: Design considerations and system implementation

Abstract: Ground-based optical telescopes, in particular large ones, require adaptive optics to overcome the atmospheric seeing limit due to turbulence. Correcting the distorted wavefront necessitates bright stars in the field of view. The sky coverage can be greatly increased by using artificial sodium laser guide stars in addition to natural guide stars. We describe the underlying physics and technical considerations relevant to such systems before discussing the design of the four-laser guide star facility (4LGSF) which is currently under development for the ESO Very Large Telescope (VLT) on Cerro Paranal, Chile. The focus is upon the justification of the requirements and their technical solution.

Keywords: adaptive optics; adaptive optics facility; ELT; laser guide star; 4LGSF; mesospheric sodium.

DOI 10.1515/aot-2014-0025
Received March 25, 2014; accepted May 9, 2014

1 Introduction

Laser guide star (LGS) adaptive optics can enable large ground-based telescopes to observe near the diffraction limit in the optical and infrared wavelength regimes anywhere in the sky. Optical turbulence in the lower 15–20 km of the atmosphere distorts incoming light from a science object. The emitted wavefront from a sufficiently bright guide star within the field of view of the telescope, whose light passes through the same turbulence as the science object, can be measured with wavefront sensors and analyzed by an adaptive optics (AO) system [1, 2]. A correction signal is sent to a deformable mirror to correct and flatten the wavefront on atmospheric timescales that are on the order of one to several milliseconds.

There is a lack of sufficiently bright stars in the sky that can serve as natural guide stars (NGS) for AO. Therefore, one has to resort to artificial beacons that can be generated by powerful lasers. The telescope includes wavefront sensors that either image the Rayleigh scattering of those lasers (Rayleigh LGS) or else the resonant scattering from alkali atoms in the mesosphere, typically sodium (sodium LGS).

The resolution of large telescopes without AO is limited by atmospheric turbulence (seeing-limited). In this regime, the image contrast relative to the sky background at constant exposure time becomes almost independent of the telescope diameter. When imaging the AO-corrected light from point-like distant objects in the diffraction limit, the dependence of the size of the Airy disk on the telescope aperture results in a concentration of light in the image and a contrast varying in proportion to the square of the telescope aperture [3]. Consequently, a number of large telescopes including Unit Telescope 4 of the Very Large Telescope (VLT) are equipped with laser guide star adaptive optics systems, and the next generation of extremely large 30–40 m-class telescopes are being designed for adaptive optics from the start. Laser guide stars can greatly extend the sky coverage of these telescopes.

The idea of using adaptive optics with artificial guide stars, produced in the mesospheric sodium layer, was first reported in classified publications by Happer and MacDonald [4] and later independently by Foy and Laberie [5] for public astronomical use. The latter paper prompted the U.S. Air Force to declassify their laser guide star AO work, performed in the 1980s and 1990s [6–8]. These early publications on LGS-AO technologies and the results marked the start of a more widespread investigation and deployment of this technique for astronomy.

***Corresponding author: Ronald Holzlöhner,** European Southern Observatory (ESO), Karl-Schwarzschild-Str. 2, 85748 Garching, Germany, e-mail: rholzloe@eso.org
Domenico Bonaccini Calia, Wolfgang Hackenberg, Steffan Lewis and Thomas Pfrommer: European Southern Observatory (ESO), Karl-Schwarzschild-Str. 2, 85748 Garching, Germany

www.degruyter.com/aot

The first non-military sodium laser guide star systems for astronomy were truly experimental systems, installed in the 1990s [9–11]. Built on this initial experience, there is a range of sodium LGS systems used for routine astronomical science operation today, most employing a single laser beam and most of them using short pulses; see [12] for a summary. A notable sodium LGS system with multiple beams (five) is the GeMS multiple LGS system at Gemini South, commissioned in 2012/2013 [13]. Another multi-LGS system, the four-laser guide star facility (4LGSF) currently under development for installation on UT4 of the VLT [14], is the subject of this article.

The remainder of this paper is organized as follows: Section 2 discusses the laser beam of guide star systems and its interaction with the sodium layer. Section 3 includes an overview of existing LGS laser source types, Section 4 presents the design of the 4LGSF, and finally, Section 5 contains an outlook of future LGS technology.

2 Optical interactions affecting the laser guide star

2.1 Sodium layer and guide star geometry

The upper mesosphere and lower thermosphere (MLT) below the ionosphere extending from 80 to 120 km provides favorable conditions for atomic metals to exist in relatively high abundance, yet at still traceable fractions (order 10^{-8} compared to the number of air molecules at this height). Such elements are deposited by micrometeorites from space that ablate in the thermosphere and subsequently recombine with electrons from the ionosphere [15]. The average sodium abundance in meteorites is about 0.6%, and while drifting downwards, the increasing air density at around 80 km allows sodium combining with oxygen radicals from ozone molecules to form sodium hydroxyl and other molecules. This lower end of the atomic sodium layer is usually defined by a sharp boundary, which points to a fast reaction rate when the air density reaches a critical limit [15]. The sodium dissipation rate is also strongly affected by the MLT temperatures, which are in the range of 180–200 K representing the coldest region in the atmosphere. Because the temperature of the MLT varies seasonally and with latitude, this lower boundary varies in extreme cases by 10 km, but usually lies between 80 km and 85 km [16].

Figure 1 shows an example of the sodium layer cross section as detected by a high-resolution lidar (light detection and ranging) system, located near Vancouver, Canada, at the University of British Columbia (UBC) Large Zenith Telescope [17]. The horizontal axis shows the time evolution, while the vertical axis is the height, starting at 75 km above mean sea level (MSL). The color represents the detected raw photon counts; see [16] for more details on the sodium layer.

The lasers of an LGS AO system excite the atomic sodium, resulting in resonant scattering of photons at a wavelength of 589.159 nm. The large product of abundance and scattering cross section makes sodium the technically most interesting alkali in the MLT.

The detected aberrations of the returned LGS wavefront that have been induced by propagating through

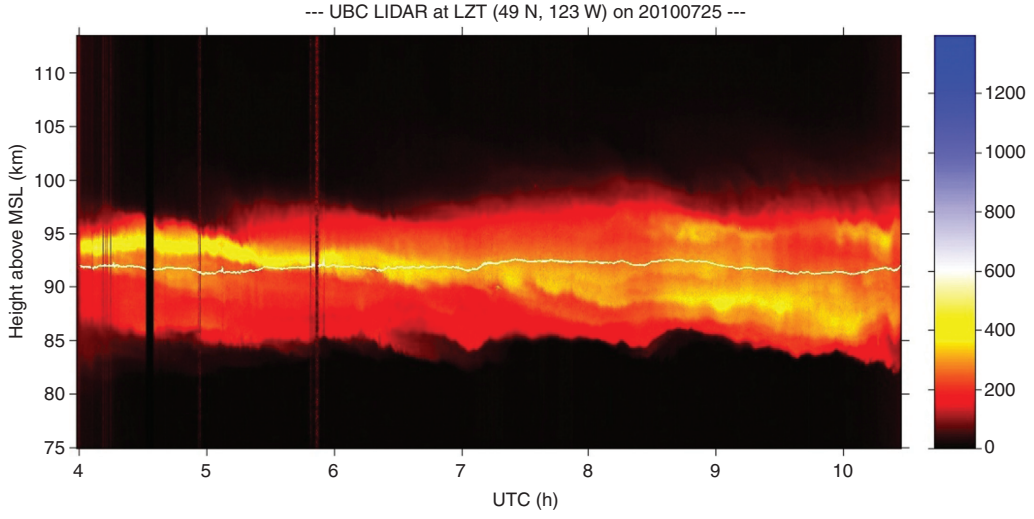

Figure 1 Example of a sodium layer detected with the UBC (UTC−9h) lidar during 1 night.

the lower atmosphere enable the AO system to acquire a real-time snapshot of the turbulence and mitigate it. The low frequency (timescale seconds) focus term of the turbulence is usually sensed with the help of one or several NGS, while the high frequency terms are sensed with the LGS signal.

If the variations in the sodium centroid are sufficiently large on small timescales (subseconds to milliseconds), they cause a performance loss of the AO system, because the usually fainter NGS signal takes longer to provide the true focus information. In the wavefront sensor signal, variations of the sodium centroid cannot be distinguished from focus variations arising from atmospheric turbulence. The resulting performance degradation of LGS AO systems may be relevant for extremely large telescopes, as the focus indetermination grows with the square of the telescope aperture D [18]

$$\sigma_{Focus} = \frac{D^2 \cos\chi}{16\sqrt{3}(a - a_0)^2} \Delta a, \quad (1)$$

where σ_{Focus} is the rms wavefront error due to focus variations Δa for the sodium centroid at altitude a, using a telescope at altitude a_0 pointing at zenith angle ζ.

From sodium profile measurements, done recently at high temporal resolutions at the LZT telescope [16, 19], the centroid height power spectral density statistic has been derived. The degree to how much the detected centroid variations affect the AO system depends on the specific AO system, see [16] for more details. For an 8 m telescope, every meter of erroneous sodium centroid height estimation causes only 0.3 nm of focus wavefront error, if not corrected otherwise with natural guide stars which is an insignificant effect. However, for 40 m class telescopes, this wavefront error increases by a factor of 25 and becomes an important contributor to the wavefront error (WFE) budget [20]. It is therefore advantageous to measure the sodium centroid location independently, and in real time, at telescopes with apertures much larger than 8 m [21].

If the illuminated resonantly scattered cylinder (LGS plume) in the sodium layer is imaged with an optical system having its pupil coaxial with the pupil of the laser launch telescope (LT), it appears as a circular spot; however, if the two pupils are laterally decentered, the LGS image appears elongated proportionally to the decenter distance. This is the case, e.g., for the subapertures of a Shack-Hartmann wavefront sensor, fed by a large telescope.

Depending on the extent of the LGS image elongation, there is a reduction of the accuracy with which the centroid can be estimated in the elongation direction. Moreover, the sodium centroid depends on the internal structure of the sodium layer and fluctuates rapidly, adding an error term in the reconstruction of the wavefront.

Figure 2 shows an example of an elongated LGS plume generated by the 5 W sodium LGS on UT4 of the VLT, observed at a distance of 2.3 km from the launch telescope. The angular extent of the LGS plume in this example is about 14 arcmin.

Because the sodium layer at about 90 km height is not at virtual infinity like the science objects, the light cone, captured by the primary mirror, does not probe the full cylinder in the turbulent atmosphere that the starlight has to pass to reach the telescope pupil [22]. This effect is called the cone-effect and can be overcome by deploying more than one laser guide star. Projecting multiple LGS in an asterism around the science field allows the AO system to cover the entire cylinder, i.e., determine the 3D atmospheric turbulence and mitigate it with the use of several deformable mirrors, each one conjugate to a turbulent layer at a different altitude [23, 24].

Multiple lasers can be launched from the side of the primary mirror or from behind the secondary mirror. The former location has the principal advantage of allowing easier access to the lasers and launch equipment, while not having to generate or relay high power laser light behind the secondary. The latter location has the advantage of requiring a smaller wavefront sensor field of view due to the smaller elongation of the imaged LGS plume since the subapertures are spaced at most by half the telescope diameter from the LT. By contrast, for the side launch configuration the spot elongation over the full primary mirror diameter applies for some subapertures. However, the center launch configuration suffers from increased background light and crosstalk onto different LGS wavefront sensors due to more Rayleigh and Mie-scattered defocused light from the uplink beams, known as the fratricide effect [25]. Using appropriately pulsed lasers and range-gating the receivers can mitigate this problem

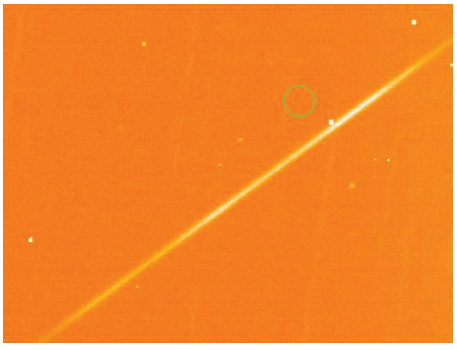

Figure 2 LGS plume imaged from the side.
The brightness variation along the line shows the sodium profile.

in principle. For the wavefront sensing on the VLT, the elongation effect is of limited importance, even in the side launch configuration.

A study of 3 years' statistics from 2008 to 2010 finds the mean sodium centroid height above sea level to be 90.8±0.1 km [16]. It extends on average over a width of 13.1±0.3 km for the range containing 95% of the photons. These values represent a mean value averaging over seasonal and nightly variations. On the wavefront sensor, this width causes a spot elongation of 0.33 arcsec per meter from the laser beam, which can add up to 13 arcsec elongation and more for a 40 m telescope! Sometimes, the layer thickness grows to as much as 21 km. The lower sodium edge was detected to lie on average at 81.7 km, and the upper edge, defined to be at five standard deviations above the local background, was found at 104.9 km. The power spectral density variability of the sodium centroid could be well represented by a power law with slope –1.87±0.02 and amplitude of 34±6 m^2/Hz which is significantly steeper than expected from the Kolmogorov theory, which would estimate a slope of –5/3 [19]. Thus, not only turbulence but also overturning gravity (buoyancy) waves play a role in the overall weather dynamics in the MLT [26].

A comprehensive study has been carried out using geophysical lidar data, albeit collected at much smaller time resolution, over 30 years by the Brazilian National Space Research Institute in São José dos Compos, São Paulo, and analyzed by Moussaoui et al. [27]. The latitude difference between São Paulo and Paranal Observatory is only one degree; therefore the statistical results are highly relevant for telescopes in northern Chile. The study found an average centroid height of 91.8 km with a standard deviation of 1.2 km and the average sodium layer width for this long-term data set was determined to be 11.2 km with a standard deviation of 1.8 km. One has to be careful when comparing these two results: The UBC data intentionally did not correct for the geometric solid angle for an observer on the ground, and thus the sodium density in the lower (upper) region of the sodium layer appears enhanced (reduced). This enhancement is, however, also seen by the LGS wavefront sensors and therefore is the relevant quantity for AO.

Statistical variations in the sodium profile centroid can be studied by analyzing its temporal power spectrum. Davis et al. [20] have made initial estimates using existing lidar data with 3-min time resolution, corresponding to frequencies below 10 mHz. The resulting power law, if extrapolating over three to four orders of magnitude into the time regime of LGS AO systems, would significantly contribute to the variance in the wavefront error [18]. A lidar experiment at the UBC at northern latitude of 49° at the 6-m Large Zenith Telescope in collaboration with the thirty-meter telescope project (TMT) and ESO has therefore been started to close this gap and collect sodium variability data at 50 Hz [19]. In addition, experiments on sodium layer statistics have been carried out at Cerro Pachón in Chile and are summarized in [13]. Good agreement has been shown between these two sites, located at very different latitudes.

The sodium layer structure varies not only with time, but the mesospheric weather also causes profile variations on horizontal scales of a few tens of meters (one arcmin at 90 km distance corresponds to 27 m), thus within the lateral separation of typical LGS asterisms [28, 29]. These differential profile variations add a focus error term to each laser guide star in an asterism and complicate the multi-laser guide star AO even further.

2.2 LGS beam propagation

The laser beam is projected by a laser launch telescope, which is essentially a high precision beam expander with an output diameter of a few tens of centimeters. Since maximizing the signal-to-noise ratio (SNR) in the wavefront sensor requires a small LGS spot size, the wavefront error of the projected beam shall be limited and the intensity profile shall be Gaussian to allow near diffraction-limited propagation. There are two widely held misconceptions about laser beams for Na laser guide stars: a) Larger LT beam diameters are generally able to generate a smaller spot size because they allow smaller waist diameters and b) it is always possible to place the beam waist at the sodium centroid by refocusing the beam.

The evolution of the $1/e^2$ beam radius in intensity $w(z)$ in a Gaussian beam is given by [30] as:

$$w(z)=w_0\left(1+\left(\frac{z}{z_R}\right)^2\right), \tag{2}$$

where z is propagation distance, w_0 the beam waist radius [hence the minimum of $w(z)$], and $z_R=\pi w_0^2/\lambda$ the Rayleigh range. When solving for w_0, one finds that the maximum distance z between waist and the launch location is limited to $z_{max}=\pi w z^2/2\lambda$. This distance amounts to 86 km for a 50 cm class LT, as in the case of the ESO single laser guide star facility ($2w$=36 cm with an LT diameter of D=50 cm) currently operating at UT4 of the VLT. For a 30 cm launch telescope ($2w$=21.6 cm, D=30 cm) as in the Four-Laser Guide Star Facility currently under development for UT4,

the maximum waist distance is 31 km. With the mean altitude of the sodium layer near 90 km, the beam waist will therefore always be located underneath the layer, so that the beam already diverges when it illuminates the sodium. Both a larger and a smaller launched wavefront curvature will shift the beam waist even closer to the LT. In practice, the effect of optical turbulence will tend to move the effective beam waist yet closer to the LT and increase the divergence [31]. The optimal wavefront curvature at the LT for minimum spot size is thus a tradeoff, depending on zenith angle and seeing.

Numerical Monte Carlo simulations of the propagation of aberrated LGS beams have been described in [32], based on the angular spectrum propagation method in which the turbulent atmosphere is modeled by discrete phase screens. The uplink propagation of a typical LGS laser beam takes place in the moderate near field (the Fresnel number equals about 2.5) and thus diffraction effects cannot be neglected. Some results are summarized below.

If the launched beam diameter $2w$ exceeds the Fried length r_0 at 589 nm (the distance along a wavefront over which the rms WFE due to atmospheric turbulence amounts to 1 radian, e.g., r_0=15 cm at zenith under a seeing of s=0.8 arcsec and 8.2 cm at s=1.5 arcsec, respectively, seeing measured at 500 nm and zenith), the Gaussian beam spawns off speckles close to the main spot. The long-exposure LGS point spread function (PSF), i.e., the mesospheric plume image blurred by the downlink seeing, gives rise to a pedestal so that the PSF begins to deviate from the PSF of a natural star in bad seeing conditions. Also, the median short-exposure spot size seen on the wavefront sensor is increased due to turbulence and, in general, the diameter of the launch telescope allowing for the lowest spot sizes will become larger the better the seeing is [32], figure 5). The simulations further show that at s=1.5 arcsec, an LT diameter of D=30 cm is optimal, while at s=0.6 arcsec, the optimal diameter lies near D=50 cm, as shown in Figure 3. In the latter case, the penalty for using a D=30 cm LT is about 0.1 arcsec for instantaneous WFS spot size. This increase seems acceptable; in particular for ELTs, considering that the WFS spot size is mostly driven by spot elongation rather than uplink spot size, especially in the side launch configuration. Furthermore, the optical aberrations in LTs with smaller diameters are generally easier to limit; besides, there is a cost benefit of smaller optics.

The simulations further show that the laser spot diameter in the mesosphere grows about linearly with propagation distance in the range of 90–180 km (the distance range to the sodium layer from 0° to 60° zenith angle of the telescope), thereby keeping the angular size seen from the ground roughly constant.

It is also instructive to analyze the wavefront aberration modes induced by the uplink turbulence. Assuming a Kolmogorov turbulence power spectrum, 90% of the mean squared wavefront aberration is contained in the tip/tilt modes and a further significant portion of the remainder is due to low-order modes such as defocus, spherical aberration, coma and astigmatism [1]. Currently operating or planned LGS-AO systems therefore include jitter compensation mirrors in the LT or in the WFS path to stabilize the LGS on the WFS field of view. If a small number of additional modes are compensated in the uplink, the mesospheric spot size can be further reduced [33]. However, to the best knowledge of the authors, LGS uplink correction

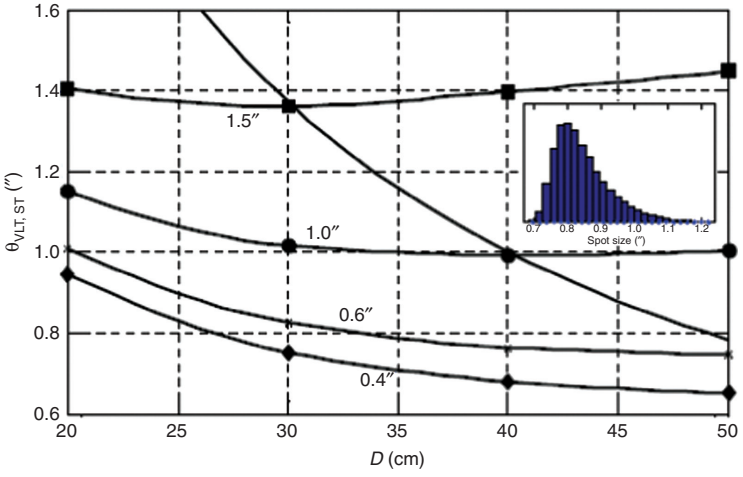

Figure 3 Median instantaneous spot size on the WFS vs. LT diameter D for different seeing values. The unlabeled curve connects the minima. Inset: Spot size histogram over time [32].

beyond tip/tilt is currently not being employed at astronomical telescopes in routine observations.

2.3 LGS return flux

Building stable, reliable lasers with several watts of average beam power at 589 nm is difficult and expensive. It is therefore important to optimize the received return flux on the ground per uplink laser power. In addition, a highly efficient laser generates less scattered light and thus ultimately delivers a better SNR, which is an added benefit of a highly efficient laser. Simple geometrical considerations yield the following formula for the return flux, Φ, on the ground (unit: photons/s/m^2)

$$\Phi = \frac{P\, T_a^{2X}\, C_{Na}\, s_{CE}}{X\, H^2}, \tag{3}$$

where P is the launched laser power in air (which is lower than the nominal laser power at the output of the laser housing), T_a is the one-way atmospheric throughput at 589 nm at zenith, X=1/cos(ζ) is the air mass at the zenith angle ζ, C_{Na} is the vertical column abundance of sodium atoms (unit: atoms/m^2), H is the vertical height of the sodium centroid above the telescope, and s_{CE} is the overall fluorescence efficiency of a laser beam exciting the sodium layer in a given pointing direction [34].

Although the line-of-sight distance between telescope and the laser spot in the sodium layer equals XH, and thus the solid angle that the receiver subtends as seen from the sodium centroid is proportional to $(XH)^{-2}$, the air mass appears in the denominator only linearly, because the slant length of the illuminated plume and hence the number of illuminated atoms scales like X. At the median sodium column abundance of 4×10^{13} atoms/m^2, only about 4% of the laser photons excite a sodium atom and thus we can consider the layer as optically thin. Equation 3 is of course only a simplification and we refer the reader to [35] for further details on the accurate return flux calculation.

All of the atomic physics governing the light-atom interaction in Eq. 3 is wrapped into the term s_{CE} and the laser must be engineered so as to maximize this quantity. First investigations of the light-atom interactions aimed at sodium LGS were carried out in the late 1990s [36]. Further studies with Monte Carlo simulations and a simplified model of the sodium atom were undertaken to understand the different return fluxes reported by the observatories [37]. A more rigorous treatment of the light-atom interactions, based on quantum mechanics and Bloch equations for the physical and environmental conditions of the mesospheric sodium, was developed in a collaborative effort between ESO and the University of Berkeley Department of Physics [34], building upon the AtomicDensityMatrix simulation package by Rochester [38].

Exciting the sodium atom such that it may emit a photon back to the telescope requires lifting it up from one of its two ground states to an excited state, followed by a spontaneous decay that emits a photon in a random direction. The two hyperfine structure ground states D_{2a} and D_{2b} are separated by 1.772 GHz and have relative strengths of 5:3. At the mesospheric temperature of about 180 K, the two transition lines are Doppler broadened to 1.07 GHz so that they partly overlap, as shown in Figure 4.

The ground and excited hyperfine states of the sodium atom are further distinguished by their magnetic quantum number, m. Exciting the atoms with circularly polarized light changes m by ±1 and repeated rapid re-excitation pushes the sodium atoms into the states with maximal (or minimal) values of m whose associated allowed transitions enjoy the largest cross sections, a process known as optical pumping [39]. In addition, the directional emission of those transitions is shaped like a figure 8, i.e., the return photon is preferentially emitted under a small angle to the laser beam and thus more likely detected.

We have run numerical simulations based on the density matrix method [34]. The code is publicly available. Our results show that the value of s_{CE} for a 20 W class CW laser becomes highest if the laser bandwidth is below 10 MHz, tuned to the center of the D_{2a} transition at a vacuum wavelength of 589.159 nm. In addition, the laser spectrum should include a second line at the D_{2b} transition center 1.713 GHz towards the blue with a power fraction of about q=12% of the total laser power to avoid the depletion of the upper (D_{2a}) ground state, a technique called repumping. The frequency difference

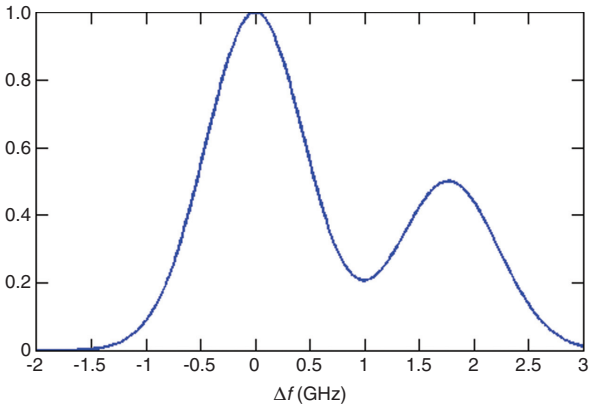

Figure 4 Relative cross-section of sodium atoms at 180 K relative to the center of the D_{2a} line.

of 1.772 GHz–1.713 GHz=59 MHz is due to selection rules that forbid direct excitations from the D_{2b} ground states to some excited states accessible from the D_{2a} ground states. Because a narrow-band laser is only resonant with a small portion of the atoms (a so-called velocity class 10 MHz wide, containing about 1–2% of all Na atoms), the repumping frequency offset must be accurate to about ±5 MHz.

To quantify the above considerations, we consider the specific return flux Ψ in units of photons/s/sr/atom/(W/m²), hence the return photon flux per uplink photon flux in the mesosphere, for a single-frequency CW laser [34]. The quantity s_{CE} can be derived from Ψ by integration across the mesosphere. Figure 5 displays simulation results of Ψ; the red curve shows Ψ for the case of q=0 and zero angle θ between the laser beam and the geomagnetic field lines, which is strongly diminished when increasing θ (magenta curve); all results are for northern Chile. The reason for the flux reduction is the Larmor precession of the sodium atoms, causing the magnetic quantum number m to cycle at a rate of 150–320 kHz and thus thwarting optical pumping and accelerating the transition of atoms to the lower ground state. Adding some laser light in the D_{2b} line mitigates this loss in Ψ significantly (blue and green curves for q=12%). The best efficiency is achieved in the spectral irradiance range of 10–100 W/m² per velocity class.

Figure 6 shows the simulated return flux on the ground for any LGS pointing direction in the sky (P=16W launched power in D_{2a} and D_{2b}, T_a=0.84, q=12% repumping), where the contour labels indicate Φ=10⁶ photons/s/m². In accordance with Eq. 2, Φ peaks near zenith (Φ=12×10⁶ photons/s/m²) where the term T_a^{2X}/X becomes maximal. The asymmetry of the peak towards the north is because s_{CE}, which depends on Ψ, varies with θ, and the geomagnetic

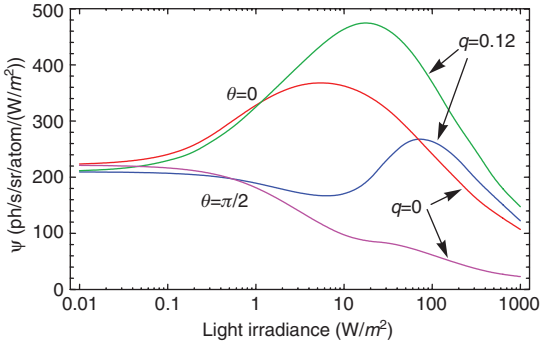

Figure 5 The specific return flux Ψ per sodium atom and laser irradiance for different angles θ between laser beam and geomagnetic field lines and the laser power fraction q in D_{2b} in northern Chile.

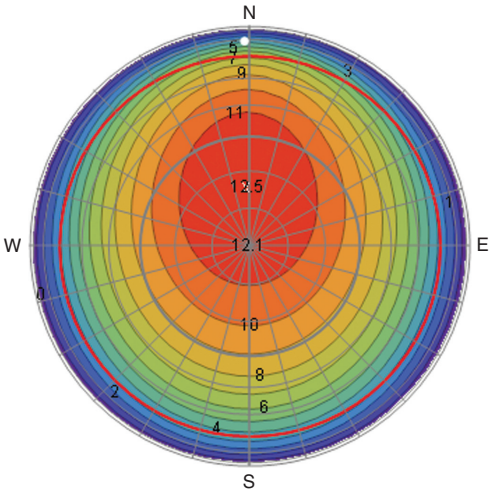

Figure 6 Simulated return flux for all possible pointing directions on sky in northern Chile (10⁶ photons/s/m²); red circle: 60° zenith angle.

field lines are inclined by 21° to the ground facing north, as indicated by the small white dot near the upper edge of the diagram. As evident from Eq. 2 and Figure 6, the brightness distribution of an LGS versus pointing differs significantly from that of a natural star (the latter scaling like T_a^X), which is one of the reasons why the often quoted equivalent V-Band LGS magnitude is not an ideal quantity to characterize LGS return flux.

We have run some on-sky experiments near Ottobeuren in Germany that have given very encouraging results [40]. However, we could only obtain data on five different photometric nights, which is too small a statistical sample to either confirm or refute the simulation results, given the known sodium layer density variability and the lack of an independent measurement of sodium abundance. Specifically, we have measured a return flux of more than 16×10⁶ photons/s/m² near zenith on some nights which agrees with our simulations for an assumed sodium column abundance of 4×10¹³ atoms/m² (we note that the magnetic field lines are inclined against the ground more steeply in Europe than in northern Chile, causing the return flux to peak more strongly near zenith than shown in Figure 6). However, we have also performed series of flux measurements and toggled between D_{2b} repumping on (q=0.12) and off so that the return flux ratio should be independent of the abundance. We have found flux ratios of 1.43 (1.44) when the light was approximately circularly (linearly) polarized, compared to simulated ratios of 1.49 (1.48). The measured flux ratio of circular to linear polarization at q=0.12 at zenith was 1.7 vs. 1.9 simulated. Further experiments are required and planned.

3 Laser sources at 589 nm

As discussed in Section 2, laser sources for sodium laser guide stars require a demanding combination of spectroscopic precision and high average power, while operating in the challenging environmental conditions at major astronomical observing facilities that are often located on mountain tops in remote locations. The main optical parameters that need to be controlled include: wavelength (resonant with the sodium D_2 transition and tunable), linewidth and lineshape, polarization state, optical wavefront quality and output power. The difficulty is compounded by the fact that 589 nm does not coincide with a natural emission wavelength for common solid-state laser media. As a result, several different laser technologies have been developed over the years. Table 1 lists a selection of telescopes with sodium laser guide stars and gives some information about the type of laser source, format and method of beam delivery that they employ.

Dye lasers were installed in a number of early LGS-AO systems [41, 44, 52]. A pulsed laser format and a free-space beam delivery were used on the Shane telescope [41] and Keck II [43] to deliver lasers with average powers of around 10–12 watts. A CW dye laser delivered via an optical fiber was employed on the ESO Very Large Telescope [45].

Beam transfer optical systems based on both free-space and optical fiber have been used in operational systems. Free space beam transfer is well suited for lasers with high peak power and has been used in the majority of installed systems to date. The upgraded VLT laser guide star facility, on the other hand, employs a 14 μm core single-mode photonic crystal optical fiber to deliver around 7 W CW output power to a launch telescope behind the telescope secondary mirror [45] that has the advantage that it maintains the diffraction-limited optical quality of the beam and simplifies the relay system. It does, however, limit in the VLT 27 m fibre relay the power spectral density to around 3 W per 100 MHz bandwidth, due to a nonlinear optical effect called stimulated Brillouin scattering (SBS) in the relay fiber. Transmission of powers greater than 3 W requires some degree of spectral broadening to be applied that reduces the return flux efficiency of narrow-band lasers. Subaru Observatory also uses an optical fiber to relay the power behind the secondary mirror [49]. This system uses short pulses and it does not suffer from SBS, although spectral broadening occurs naturally in the optical fiber due to another nonlinear optical effect called four-wave mixing.

Another important group of lasers is based on nonlinear sum-frequency generation (SFG) using the combination of two laser wavelengths at 1 064 nm and 1 319 nm that are natural transition wavelengths of the Nd:YAG laser crystal. Such SFG schemes can emit CW or pulsed light and they are typically solid state lasers based on free-space optical designs. Examples of SFG lasers are the Starfire Optical Range that reported CW optical powers of greater than 50 Watts in an output spectral line having a linewidth of less than one MHz [51]. The recently installed laser system at Gemini South [43] employs a 50 watt pulsed SFG laser whose beam is split to form five individual LGS at the end of a free-space beam relay. Work is also ongoing to apply a novel SFG approach pumped by an Nd-doped fiber laser at 938nm [53] and a commercial 1583 nm fiber laser [54].

In recent years, ESO has undertaken laser developments with prototypes [55] for the planned VLT Adaptive Optics Facility (AOF) [56]. The laser uses a newly patented approach [46, 57] that employs Raman optical fiber amplifiers and a master oscillator power amplifier (MOPA) configuration. The last prototype laser of this type was deployed at the VLT under the name PARLA in a recent upgrade of the Laser Guide Star Facility [47]. This new laser technology is used in the 4LGSF together with a free-space beam delivery as described later in this article.

Table 1 Laser formats and beam delivery types of some LGS systems.

Institution/telescope	Type of laser source	Format	Beam delivery	References
Lick/Shane	Dye laser	Pulsed	Free space	[41]
Keck I, Gemini South	Solid state sum frequency	Pulsed	Free space	[42, 43]
Keck II	Dye laser	Pulsed	Free space	[44]
ESO/VLT	Dye laser	CW	Optical fiber	[45]
ESO/VLT upgrade	Raman optical fiber laser	CW	Optical fiber	[46, 47]
Gemini North	Solid state sum frequency	Pulsed	Free space	[48]
Subaru	Solid state sum frequency	Pulsed	Optical fiber	[49]
Palomar	Solid state sum frequency	Pulsed (micro/macro)	Free space	[50]
Starfire Optical Range (SOR)	Solid state sum frequency	CW	Free space	[51]

4 Instrument example: the 4-Laser Guide Star Facility

4.1 Laser guide star unit: system description and overview

The 4LGSF [14] is part of the Adaptive Optics Facility (AOF) [56], which is planned to be installed on UT4 of ESO's VLT on Cerro Paranal. The AOF is a ground layer adaptive optics system aiming at correcting a wide field of view using information from natural guide stars for low-order correction, as well as the return flux from laser guide stars produced by four high-power lasers tuned to the sodium resonance wavelength for high-order corrections.

The 4LGSF consists of four LGS units (LGSU), each unit being able to produce independently one laser guide star. Each LGSU is capable of launching a 30 cm collimated laser beam towards the sodium layer with an average power ≥17 W in air. The optical throughput of each laser guide star unit is designed to be > 88%. The LGSU consists of a laser source and a launch telescope system (LTS), plus control electronics and software.

Optomechanically, the LTS is composed of two main-line replaceable units, the beam conditioning diagnostic system (BCDS) and the optical tube assembly (OTA), optically arranged as in Figure 7, and mounted as shown in Figure 8. The laser head is mounted directly onto the BCDS. The laser, BCDS and OTA are mounted on a steel baseplate, which is aligned in tilt with respect to the UT4 optical axis during integration.

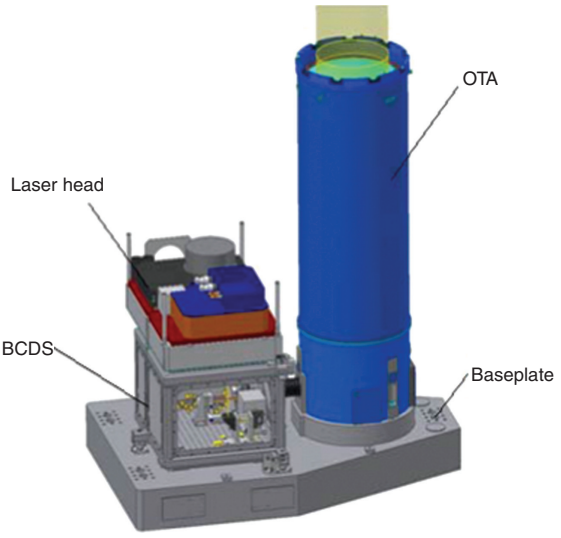

Figure 8 LGS unit assembled on the support baseplate. The laser head is mounted on top of the BCDS, which is bolted on the steel baseplate next to the OTA.

The OTAs have been manufactured by TNO in Delft, Netherlands, adopting the ESO reference optical design [58]. The beam expanders of the BCDS were manufactured by Optec S.r.l (Parabiago, Italy). In the LTS subunits, a 4.8 arcmin radius (on sky) field steering mirror, a fast LGS jitter control mirror, and a focusing unit are accommodated.

The LGSU are mounted on the UT4 altitude structure and move with it. Therefore, the LGSU has to be stable against gravity vector changes and environmental variability such as thermal changes in the range of 0–15°C. The modular design allows the failure of one complete LGSU to be tolerated with the AO system running in a degraded but workable mode. In addition, all subsystems are designed to be interchangeable line replaceable units (LRU), allowing for efficient, fast corrective maintenance with minimal downtime of the system. Since the multi laser guide star system is designed for a lifetime of ten years or more, a modular system design and redundancy are needed to achieve the required availability. A wind cover protects the LGSU and a dust cover shutter protects the aperture of the launch telescope through a baffle tube in order to limit the solid angle of the cold sky that the exit lens of the OTA sees.

The laser source that was selected, based on ESO patented Raman fibre technology, enables the 4LGSF to be run in an observatory environment by reducing the need for maintenance due to its high reliability and more simple operation compared to existing laser guide star facilities. The control electronics cabinet, together with the laser

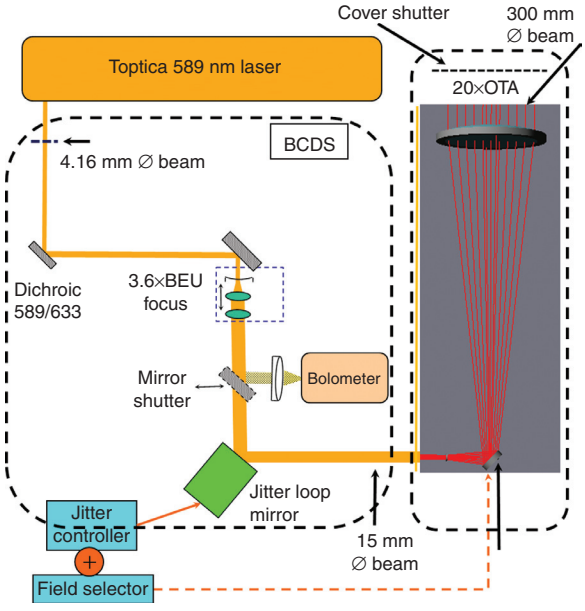

Figure 7 4LGSF LTS layout with BCDS and the OTA subunit. The BEU focusing lens, the mirror shutter, the jitter loop mirror, the OTA field selector mirror and the cover shutter are motorized.

head, are both mounted on the centerpiece of telescope, reducing the cable length between the subsystems. The laser source subunits are being manufactured, under contract and ESO technology license, by Toptica Photonics GmbH of Munich, Germany and MPB Communications Inc. (Montreal, Canada) and they are described [59].

The optical path from the laser source to the launch telescope exit lens is very short. Cumbersome, complex laser beam delivery systems are hereby avoided and the systems reliability and simplicity is increased. A stiff honeycomb steel baseplate hosts the entire laser guide star unit with its several optical subsystems; suitably lightweighted for its location on the moving centerpiece of the VLT and insensitive to temperature transients.

The alignment philosophy of the LTS follows a modular scheme based on line replaceable units. It is such that each LRU subsystem alone (laser head system, BCDS subsystems, and OTA) is aligned internally separately. Precise optomechanical references on each subsystem then enable the complete laser guide star unit to be assembled out of the pre-aligned subsystems. This AIT approach has been addressed in the mechanical design from a very early stage of development by properly selecting the type/shape of optimal mechanical interfaces and alignment means.

The laser heat exchanger and two electronics cabinets, responsible for the entire 4LGSF safety interlock, housekeeping and control software aspects are not on the centerpiece but on the azimuth structure below one of the two UT4 Nasmyth focus platforms; see Figure 9.

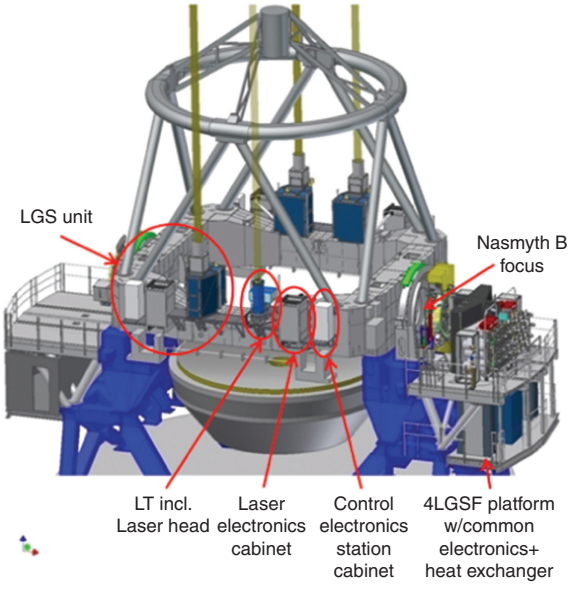

Figure 9 Four LGS units mounted on the VLT UT4 Centerpiece. The wind protection cover has been removed from one LGSU; note also the electronic cabinets on the 4LGSF platform, located under the Nasmyth B focus.

4.2 4LGSF system requirements

For routine operation of LGS-assisted AO at astronomical observatories, the requirements for the facility generating the artificial stars are very similar to those of the astronomical telescope infrastructure itself regarding operability, maintainability and availability. The technical downtime of the telescope due to preventive or corrective maintenance shall be less than a few percent of the total observation nights per year. Since the number of observing nights at good sites is in excess of 300 per year, a high reliability of the laser guide star facility and its subsystems is mandatory. Automatic health checks of the laser guide star system, executed during day-time, are a part of the maintenance approach needed to meet this level of availability. The operation of the multi laser guide star system also has to be fully automatic in order to reduce overhead during laser startup or the acquisition of the laser guide stars by the AO system after an observation target preset. The 4LGSF main system level requirements are:

- The 4LGSF LGSU shall be controllable simultaneously and independently of each other.
- Each of the four LGS beams shall be projected from a launch telescope system located at the VLT-UT4 centerpiece.
- The 4LGSF may receive from the client AO system the command to toggle on and off the Na D_2 line by 5 GHz.
- The laser beam propagated to the mesosphere shall be circularly polarized.
- The LGS return flux when pointing at zenith under median sodium abundance is at least 7.7×10^6 photons/s/m^2.
- Actuators to control the focus of each of the launched laser beams shall be implemented in the 4LGSF. The 4LGSF focus actuators shall accept offset requests from the AO system.
- During AO closed loop, the 4LGSF shall track the sodium layer distance changes due to UT tracking. The coarse blind focus tracking shall have an accuracy of $\leq$5 km. The 4LGSF shall inform the AO system about its focus position.
- Actuators to control the preset pointing of each of the launched laser beams shall be implemented in the 4LGSF. The 4LGSF preset pointing actuators shall accept offset requests from the AO system.
- Actuators to control the fast angular uplink jitter of each of the launched laser beams shall be implemented in the 4LGSF.

From the considerations discussed in Section 2, the following requirements have been derived:

For a required return flux of 7.7×10^6 photons/s/m^2 on the ground at Paranal at a median sodium column density of 4×10^{13} atoms/m^2 and pointing at zenith, a CW laser with a linewidth <10 MHz, a propagated beam power $P\geq17$W, 10% of which are emitted in the D_{2b} repumper line, with 95% of the emitted light circularly polarized, fulfills the requirement. These requirements are in accordance with the arguments and simulation results presented in Subsections 2.2 and 2.3, taking into account a spectral irradiance of ≈50 W/m^2 per velocity class of the Na atoms (see Figure 5 in Section 2.3) when the LGS short exposure FWHM is 1.3 arcsec in diameter. The chosen laser characteristics are based on the numerical simulations that have not yet been fully validated by conclusive experiments [40].

The short exposure LGS image size on the adaptive optics WFS depend on the seeing, the turbulent layer distribution in height (C_n^2 profile), the launched beam diameter and on the wavefront errors present in the launched uplink beam. Table 2 compares the median simulated FWHM of short exposure wavefront sensor spots [32] when the LGS is pointed at a zenith angle of $\zeta=30°$, for different seeing cases (measured at 500 nm at zenith), taking into account the propagated laser beam wavefront aberrations induced by the laser and optics and the launched beam diameter D, assuming that the beam diameter at 1/e^2 intensity level w obeys $2w/D=0.72$. Using this ratio, we clip the Gaussian beam at the 2% level in intensity that is sufficient to curb diffraction and beam power loss [60, 61].

The launch telescope diameter and the required wavefront quality of the uplink laser beam, to be met under operational and environmental loads, drive the cost and complexity of the launch telescope optics. The latter is usually underestimated. Considering the AOF WFS plate scale of 0.85 arcsec/pixel, the best tradeoff between cost, return flux and launch optomechanics optical properties is given by a 300 mm laser beam diameter, with an uplink beam WFE of up to 100 nm rms.

By comparison, the turbulence induced WFE on the 300 mm diameter uplink beam is 75 nm and 125 nm rms for seeing conditions of 0.5 arcsec and 1 arcsec, respectively, assuming jitter loop corrections with a factor five suppression of the LGS jitter.

A focus actuator in the optical system is necessary to compensate for focus drifts of the launch telescope optics under the environmental loads (pressure, temperature, gravity direction), to compensate for focal plane curvature across the launch telescope field of view and for the variation of the mesospheric layer distance vs. LGS pointing altitude above the horizon, ranging from 20° to 90°. In practice, the last term is rather small, as can be seen in Figure 10, derived with physical optics beam propagation. If no focus correction is applied to compensate the variation of the LGS distance versus altitude, the angular size of the LGS changes by only ≈7% between 90 and 200 km.

The focus drift can change the size of the LGS imaged at the mesosphere. A Zernike defocus coefficient (ISO definition) residual within ±λ/10 limits the LGS nominal size increase to within ≈12%, noting that this is referred to the sole contribution of a perfect Gaussian beam propagated at the mesosphere and does not take into account the turbulence effects on spot size. To limit the environmental effects on focus, passive and active measures can be implemented, as shown in Subsection 4.4.

Table 2 Short exposure FWHM size of wavefront sensor spots for different seeing and emitted beam wavefront rms errors.

Seeing (arcsec)	WFE rms (nm)	WFS short exposure spot sizes (arcsec)		
		D=30 cm	*D*=40 cm	*D*=50 cm
		Median	Median	Median
1.0	70	1.213	1.162	1.145
0.6	70	1.013	0.911	0.862
1.0	100	1.288	1.225	1.180
0.6	100	1.099	0.983	0.913

4.3 Laser source subunit

The laser source subunits are responsible for laser beam generation, for their own thermal management and for

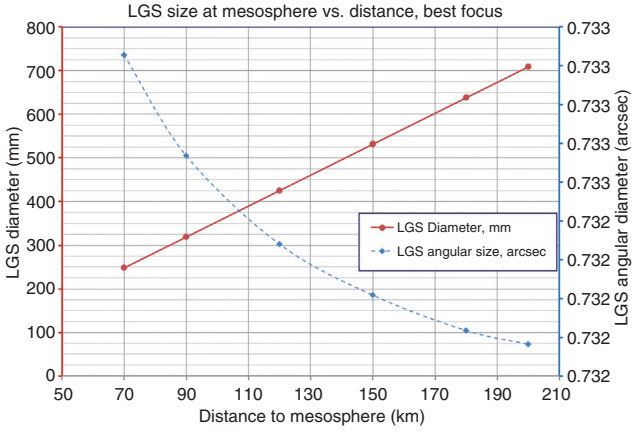

Figure 10 LGS diameter at the mesosphere, in mm (circles, left axis) and arcseconds (squares, right axis) for the best focus setting.

providing maintenance tools and ancillary equipment. There are four laser sources in the 4LGSF and these shall be modular and interchangeable to facilitate maintenance and increase the overall availability of the ensemble of four laser sources. The laser sources are mounted on the telescope altitude structure with corresponding requirements for compactness, operation in different orientations and in the daytime and nighttime environment (temperature, humidity) inside the telescope dome. The subsystem requirements for the laser sources, derived from the overall 4LGSF system design are summarized in Table 3 below.

Optomechanically the laser head has an interface with the laser projector. Requirements for the laser source output beam stability arise because beam decenter and tilt are transferred to the laser guide star pointing in the mesosphere. The tolerance on laser pointing is tight due to the narrow field of view of the LGS-AO wavefront sensors in the telescope. In addition, the maintenance approach of the system requires interchangeability between laser sources and repeatable mounting of the laser on the laser projector. The requirements for the output beam repeatability on exchange of a line replaceable unit are <100 microns lateral and <0.16 mrad tip and tilt; the output beam lateral and tip/tilt decenter are additionally required to be stable to within these same ranges during operation and over all environmental loads (gravity and temperature). The mass of each laser source is limited to less than 1 000 kg on the telescope centerpiece and an electrical power supply of 4 kVA per laser is available for normal power.

Because the lasers are mounted on the centerpiece of the telescope, the surface temperature of the equipment cannot be more than 1.5 K above the ambient temperature in the dome for temperatures between 0 and 15°C and a nighttime temperature gradient of up to -0.7 K/h to avoid creating convective turbulence interfering with science observations. The lasers shall deliver full performance for operational pointing ranges from vertical down to 20° above the horizon.

The telescope is a low-vibration environment due to the general sensitivity of optical measurements and particularly optical interferometry, precluding the use of rotating parts such as fans and pumps in equipment mounted directly on the telescope. Other requirements such as earthquake loads and compatibility with the electromagnetic environment in the UT4 enclosure also exist.

The class IV laser is controlled from the 4LGSF control system via Ethernet. The laser is required to implement a defined control interface for normal operation, maintenance and servicing of the system.

Physically, each of the four lasers comprises an electronics cabinet and a laser head; a single heat exchanger provides chilled liquid coolant for all four laser sources. The electronics cabinet and the laser head are mounted together on the telescope centerpiece separated by around two meters, with electronic, optical fiber and cooling connections running between them. The laser head has approximate dimensions of 700 mm (L)×500 mm (W)×285 mm (H) and a mass of around 65 kg. The heat exchanger is mounted on a gravity-invariant platform under the Nasmyth B platform of the telescope. It distributes coolant through the altitude cable wrap to the four laser subunits.

The power consumption of the complete laser system, consisting of four individual laser units, amounts to less than 4×1 kW, from which the power dissipated within each laser head is <100 W. Both the laser head and the electronics cabinet are equipped with thermal insulation to avoid local turbulence. The system exhibits fast, fully automatic warm-up times of the order of 30 min including startup self tests when the system temperature is maintained with continuous cooling.

Following [59], optically the 4LGSF laser consists of three main elements: a low-power seed laser having a very stable output wavelength at 1178 nm, a high power infrared Raman optical fiber amplifier, and an efficient means of frequency-doubling to generate the final yellow output wavelength as shown schematically in Figure 11. The Raman fiber amplifier (RFA) is pumped by a 100 watt-class ytterbium fiber laser at a wavelength of 1120 nm and produces an output power of up to around 40 W at 1178 nm, while preserving the spectral and polarization characteristics of the seed laser. The frequency-doubling cavity (SHG) has routinely demonstrated optical conversion efficiencies of >80% from 1178 nm to the final output wavelength 589 nm.

Table 3 Main optical requirements for the CW laser sources.

Parameter	Value	Units
Vacuum output wavelength (sodium D_2 transition)	589.159	nm
Useful output power (D_{2a}+D_{2b})	20	W
Laser power stability, long term (peak-to-valley)	≤15	%
Fraction of useful power resonant with D_{2a}	90	%
Fraction of useful power resonant with D_{2b} (D_{2a}+1.713 GHz)	10	%
Full width half maximum width of each spectral line	<250 (<5 goal)	MHz
Laser detuning range	>5	GHz
Output optical beam wavefront error (rms)	<70 (<25 goal)	nm
Polarization state	Linear	

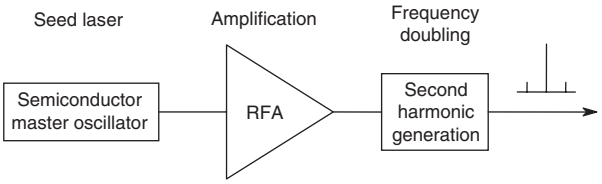

Figure 11 Schematic of the laser system adapted from [59] showing the diode seed laser, a Raman fiber amplifier (pump source not shown) and the SHG module with the repumper generation.

Spectrally, the laser output consists of a central line resonant with the sodium D_{2a} transition and containing 80% of the optical power. Two spectral sidebands, separated from the main line by ±1.713 GHz, respectively, each contain 10% of the output power. The higher frequency sideband is resonant with the sodium D_{2b} transition and is known as the 'repumper' and contributes to an enhancement of the laser guide star return flux, as shown in Section 2.

The laser is required to be able to detune the center wavelength by greater than 5 GHz for background calibration, which has been demonstrated in this laser design with tuning and detuning times of around 1 s [59]. The laser head, mounted on the laser projection subunit, delivers a free-space linearly polarized output beam having a Gaussian beam waist ($1/e^2$ in irradiance) diameter of 3 mm and the beam waist location within 2 m of the laser output interface. The Gaussian laser beam propagated has a diameter of 4.16 mm at the 2% irradiance level.

4.4 Athermal refractive launch telescope system

For the laser powers involved, a Galilean beam expander for the laser transmitter without an intermediate focus is preferred over a Keplerian design. The advantage of a refractive design is the pupil symmetry (useful for polarized beams) and lack of central obstruction, compared to off-axis or on-axis reflecting designs. Moreover, reflective launch telescopes typically need either a thick or a thin exit window of the same size as the launched beam, which re-introduce the thermal inertia and gravity load problems of the large lenses in a refractive design.

The launch telescope system (LTS) of the 4LGSF has a refractive optical design. A tradeoff study done at the beginning of the project favored a simple optical design comprising two cascaded beam expanders, one of which can vary focus. The elements with optical power are confined to the beam expanders, which are pre-assembled and tested independently, largely simplifying the alignment and tolerances in the LTS optomechanics. The first beam expander unit (BEU) applies a 3.6× magnification to the 4.16 mm beam of the laser beam input to 15 mm diameter, while the second beam expander, the optical tube assembly (OTA) applies a magnification 20×, producing a 300 mm output beam diameter, as shown in Figure 7. The $1/e^2$ irradiance level output beam diameter is 216 mm or 300 mm at the 2% irradiance level.

The chosen optomechanical design is athermalized for soaked temperatures in the range 0–15°C and for transients in air temperature at rates of up to ±0.7°C/h. Furthermore, the laser light absorption induces radial thermal gradients in the glass of the lens system (thermal lensing). Also, the radiative cooling of the exit lens, when it is suddenly exposed to the cold night sky, induces a transient thermal lens because the outer parts of the lens where the glass is thinner cool faster than the lens region closer to the optical axis. The requirements are summarized in Table 4. The output beam circular polarization requirement has drawn special attention to the quality of optical coatings regarding their reflectivity and relative phase retardance between the *s* and *p* polarization directions.

The specified maximum wavefront error of the LTS is ≤100 nm rms, to be maintained under laser load, ambient temperatures between 0 and 15°C, temperature gradients of ±0.7 K/h, and air pressures of 750±50 hPa. The wavefront error budget is shown in Table 5.

The BCDS optomechanics is based on stainless steel for the supports and high quality fused silica for the optical elements, with optical coatings made by ion beam sputtering. The optical layout of BCDS is shown in Figure 12. The beam expander optical path is 74 mm long. The OTA optical layout is shown in Figure 13. The OTA includes a quarter-wave plate to convert linear to circular polarization, followed by a negative lens working at *f*/4 optical speed. The laser beam reaches a motorized folding mirror

Table 4 Main optomechanical requirements of the LTS.

Optomechanical requirements launch telescope system	Value	Units
The laser source is hosted on board of the LTS structure	–	–
Launched laser power at the output of the LTS	17	W
Uplink beam wavefront error (rms)	≤100	nm
Uplink beam anamorphism	≤15	%
Uplink beam ratio of circular polarization vs. total intensity	≥95	%
LGS pointing angular field radius	4.8	arcmin
LGS open loop pointing absolute accuracy	±2/5	arcsec
LGS jitter tip-tilt actuator refresh rate	1000	Hz

Table 5 Allocation of the WFE budget among the LGSU subsystems.

WFE source	WFE nm (rms)	Coherent En. @589nm
Laser beam	≤70	0.57
BEU (part of BCDS)	≤35	0.87
Flat relay optics (part of BCDS)	≤20	0.95
OTA	≤50	0.75
Baffle turbulence	≤28	0.90
Total (in quadrature)	≤99.0	0.32

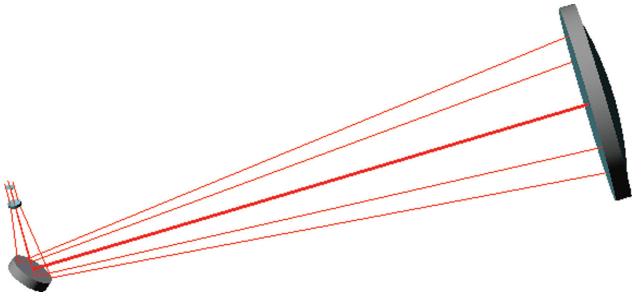

Figure 13 Optical Layout of the OTA.
Note the quarter-wave plate on the 15 mm input parallel beam, the small negative lens of the Galilean beam expander, and the 380 mm large collimating lens. The folding mirror acts as field selector.

which acts as field selector, to point the LGS within the 4.8 arcmin field of view. The positive lens in this Galilean design, 380 mm in diameter, collimates the optical beam to 300 mm and projects the LGS on the mesosphere. It is made of Schott N-BK7 of high homogeneity and optical quality.

It is recognized that using a large, thick lens can induce focus variations due to the long thermalization times of the glass. The following measures have been taken to passively athermalize the LTS:

- The BCDS mechanical components supporting the optics are made of the same material, and care has been taken in designing the mounts to avoid that differential expansions induce tilt on the supported flat optics.
- The beam expander (BEU) is athermalized by design for soaked temperatures, by a careful choice of the optical and mechanical materials of appropriate expansion and refractive index thermal coefficients. The BEU behavior under temperature transients has been analyzed, and found to cause negligible effects.
- The materials and spacers between the subcomponents are chosen to compensate the focus variation with temperature. In order to cope with the temperature transients, we analyzed the temperature and refractive index distributions using finite element methods and optical design CAD to evaluate the effects of soaked and transient temperatures on the output beam focus.

Passive methods have been implemented to cope with the transient effects, in practice adding thermal mass to the parts that change length with temperature variations to reduce thermal variations of the optics.

The following measures have been taken as baseline to actively athermalize the LTS:

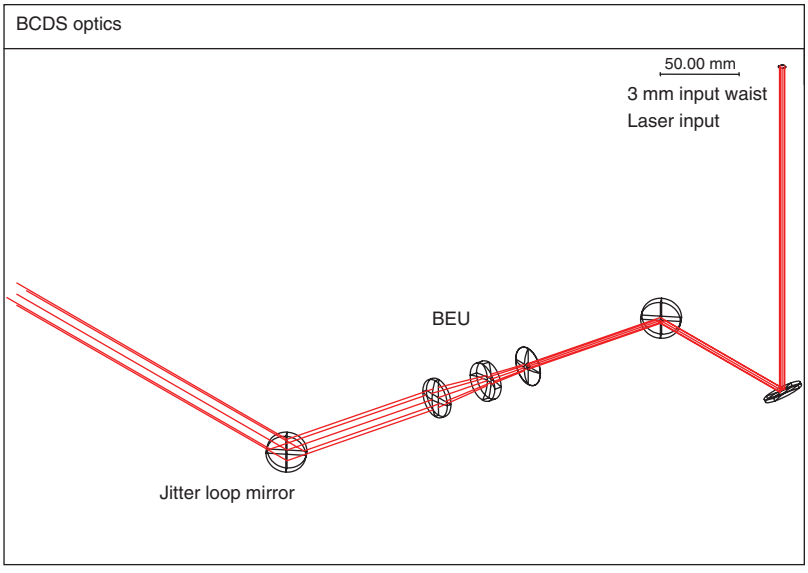

Figure 12 BCDS optics, consisting of three lenses for the BEU, one 633/589 nm dichroic and two flat mirrors. The BEU middle lens is motorized to adjust the LTS output beam focus. The BCDS controls LGS focus and jitter.

- Use temperature and pressure information for the focus actuator control. During the test phase, the LTS focus is calibrated for soaked and transient operating temperatures in a thermal chamber, using an interferometer.
- The focus calibration includes the high power illumination of the LTS optics. The time of laser illumination will be used for focus actuator control, with an experimentally calibrated model of the focus.
- The AO system measures the LGS spot size on long time averages (tens of seconds) from the WFS data and adjusts the focus actuator of the respective LGSU.

Finite element analysis and optical CAD have been used to compute the optomechanical flexures under gravity and temperature loads and the thermal gradient in the optics to estimate the thermal and gravity loads (gravity direction changes) effects during operation. The results in terms of wavefront error, LGS pointing and beam footprint shift on the OTA large lens L2 are summarized in Table 6. Note that the ΔPointing and ΔFootprint are radial values, assuming that all contributing error terms sum up with the same sign (worst case). ΔFootprint is the decenter of the output laser beam on the OTA-L2 exit surface. The laser illumination results in a shift of the focus, and is not counted here. The above results have to be validated during the integration phase. Preliminary results on the environmental load effects on the wavefront error are consistent with the analysis summarized in Table 6.

4.5 Summary

The brightness of LGS must be raised to keep step with more demanding instruments, requiring more powerful lasers, especially during periods of low sodium abundance. The 4LGSF as part of the AOF, which is under testing in Europe for installation at the 8 m UT4 of the VLT in Chile, aims at providing four bright LGS. It is a new generation of LGS facility employing four 22 W narrowband CW lasers, featuring D_{2b} repumping and a projected circular polarization state to optimize the return flux efficiency.

The challenge in the 4LGSF design is to fulfill the stringent performance requirements for operation and maintenance. The new modular design of the 4LGSF based on LGS Units provides a number of advantages. The refractive launch telescope design has prompted us to implement some passive and active measures to control the thermal effects on the focus term. The LGSU is assembled and is undergoing extensive tests in Europe.

The 4LGSF on the UT4 VLT requires a retrofit of a telescope already in operation. We believe that the 4LGSF concept with its modular LGSU units also represents a pathfinder for multi-LGS-assisted AO for 30–40 m class astronomical telescopes.

5 Outlook

The 4LGSF is designed to provide a significant step in terms of LGS brightness, ease of operation and availability. The baseline of the E-ELT telescope for LGS lasers and laser launch telescopes is comparable to that of the 4LGSF in terms of beam parameters and required return flux. The natural question arises which performance/availability risks remain and in which direction the field may evolve to solve them.

The technical objective is to achieve a sufficient signal-to-noise ratio on the wavefront sensors of large telescopes under all operating conditions such as variable guide star constellations, fluctuating sodium abundance,

Table 6 Summary of the analysis results for the environmental effects on the LTS.

	Environmental Load	ΔWFE (nm rms)	ΔPointing (arcsec)	ΔFootprint on OTA-L2 (mm)	Comment
UT4 flexure	Gravity (0°–70°)	0	25	0	From analysis
UT4 hysteresis	Gravity	0	1.8	0	Calibration
Laser	Gravity (0°–70°)	0	0.1	0.9	Provider analysis
BCDS and baseplate	Gravity (0°–70°) and T (0–15°C)	6.3	2.4	0.8	
OTA structure	Gravity (0°–70°)	5.1	2.7	0.002	
Laser	Temp (0–15°C)+dT/dt	0	0	0	Temp. controlled
OTA	Temp (0–15°C)+dT/dt	5.2	0	0	Athermalized
BCDS and Bas.	dT/dt=0.7°C/h	1	0.02	0.1	
Total	All loads	9.6	32.0	2	
Allowed values		19	60	13	

variable seeing conditions and variable sodium layer profiles. Recently built LGS systems employ multiple guide stars, all of which being observed from the entire pupil, some parts of which may be tens of meters away from the launch telescope. A diffraction-limited LT in 0.8 arcsec seeing can achieve a short-term spot size of about 1.2 arcsec suggesting a wavefront sensor plate scale of 0.6 arcsec (Nyquist sampling). Capturing 95% of the plume of a guide star that is launched 40 m away and thus elongated to 13 arcsec requires about 22×22 pixels per subaperture, in turn not only necessitating very large sensor chips, but also spreading the return flux over many pixels, causing elevated noise levels. The clipping of the plume image on a wavefront sensor is currently considered a serious problem for MCAO systems [62]. Field experiments are proposed toward an experimental assessment of the performances of AO systems with extremely elongated LGS, such as those of the future E-ELT [63].

When projecting the lasers from behind the secondary mirror instead of from the rim of the primary, the maximum spot elongation is cut in half, albeit at the expense of much more difficult installation of the launch equipment and more severe laser fratricide (wavefront sensors blinded by the beam belonging to another LGS). A further complication is focus indetermination due to fast variations of the sodium centroid height. A consequence of spot elongation is that the location of the star image centroid in the direction of the beam cannot be measured accurately; focus indetermination means that even if the centroid of the imaged plume was known, its actual height above the ground would still be uncertain [28]. Aside from technical and engineering issues, these two effects possibly present the most serious fundamental challenges to the application of multiple sodium LGS to date for the ELTs. Solutions to overcome these problems are being sought and field experiments are needed [40] to address their feasibility.

The sensing uncertainty along the beam propagation direction can be overcome in principle by pulsing the laser, or at least applying a partial amplitude modulation. If the pulse duration is small compared the laser transit time through the sodium layer (1 μs=300 m) and the pulse repetition rate small enough to ensure that there is, at most, one pulse in the layer at any time (order 10 kHz), one can do spot tracking, and also obtain enough information to deduce the layer profile similar to a lidar [64]. In order to mitigate the WFS spot elongation effect caused by the finite thickness of the mesosphere, one can either collate the return photons from different altitudes by synchronous refocusing of the wavefront sensor, known as dynamic refocusing [65] or else by on-chip spot tracking, e.g., through synchronous charge migration on a radial coordinate CCD sensor [66]. Moreover, avalanche photodiode (APD) arrays can accomplish a fully time resolved recording of the LGS pulse return, although a large number of subapertures would lead to high system complexity [67, 68].

A less demanding mitigation of spot elongation would be to partially modulate the power of a CW LGS laser using a pseudorandom bit pattern and deconvolve the time-resolved return signal with that same pattern, from which one can obtain the full layer profile, a technique that has been demonstrated on the VLT (at 100% modulation depth). This modulation would be maintained permanently in order to yield the sodium layer structure for the weighted center of gravity and matched filter centroiding algorithms [69]. An on-sky feasibility test at ≈10% modulation depth has been proposed at the 6 m liquid mirror Large Zenith Telescope near Vancouver, Canada [40].

The field of sodium LGS in ground-based optical astronomy has evolved within only 20 years from humble beginnings towards providing turn-key science production instruments. Besides work on advanced modulation and sensing schemes, further R&D towards CW and pulsed lasers with higher power, reduced size and lower cost is being carried out. The race for ever better image resolution in telescopes continues at a fast pace.

References

[1] J. M. Beckers, Ann. Rev. Astron. Astrophys. 31, 13–62 (1993).
[2] R. Davies, M. Kasper, Ann. Rev. Astron. Astrophysics, 305–351 (2012).
[3] J. W. Hardy, in 'Adaptive Optics for Astronomical Telescopes', (Oxford Univ. Press, Oxford, UK, 1998).
[4] W. Happer and G. MacDonald, JASON Report, JSR-82-106, MITRE Corp., (McLean, VA, 1983).
[5] R. Foy, A. Labeyrie, Astron. & Astrophys. 152, L29–L31 (1985).
[6] L. A. Thompson, C. S. Gardner, Nature 328, 229 (1987).
[7] R. Q. Fugate, C. H. Higgins, J. L. Wynia, W. J. Lange, A. C. Slavin, et al., Bull. Am. Astron. Soc. 23, 898 (1991).
[8] W. Happer, G. J. MacDonald, C. E. Max, F. J. Dyson, J. Opt. Soc. Am. A 11, 263–276 (1994).
[9] D. T. Gavel, S. S. Olivier, C. E. Max, H. W. Friedman, J. M. Brase, et al., Bull. Am. Astron. Soc. 25, 888 (1993).
[10] S. S. Olivier, C. E. Max, K. Avicola, J. M. Brase, Friedman, et al. Astron. Soc. Pacific 55, 82 (1993).
[11] A. Glindemann, D. Hamilton, S. Hippler, R.-R. Rohloff, K. Wagner, in 'Laser Technology for LGS-AO Astronomy', Ed by. N. Hubin and H.Friedmann (ESO, Garching, Germany, 1997) pp. 120–125.
[12] R. Holzlöhner, S. M. Rochester, SPIE Proc. 8447-17 (2012).
[13] B. Neichel, C. d'Orgeville, J. Callingham, F. Rigaut, C. Winge, G. Trancho, MNRAS 429, 3522 (2013).

[14] W. Hackenberg, D. Bonaccini Calia, S. Lewis, R. Holzlöhner, B. Buzzoni, et al., Proc. AO4ELT2 Conference Proceedings (2011).
[15] J. M. C. Plane, Chem. Rev. 103, 4963–4984 (2003).
[16] T. Pfrommer, P. Hickson, Astron. Astrophys. 565, (2014); doi: 10.1051/0004-6361/201423460.
[17] P. Hickson, T. Pfrommer, R. Cabanac, A. Crotts, B. Johnson, et al., Pub. Astron. Soc. Pacific 119, 444–455 (2007).
[18] G. Herriot, P. Hickson, B. D. Ellerbroek, J.-P. Veran, Proc. SPIE 6272-0Q (2006).
[19] T. Pfrommer, P. Hickson, J. Opt. Soc. Am. A 27, 97 (2010).
[20] D. S. Davis, P. Hickson, G. Herriot, C.-Y. She, Opt. Lett. 31, 3369 (2006).
[21] D.-J. Butler, R.-I. Davies, H. Fews, R.-M. Redfern, N. Ageorges, et al., Proc. SPIE 4007, Adaptive Optical Systems Technology, 358 (July 7, 2000); doi:10.1117/12.390318.
[22] R. Foy, in 'Optics in Astrophysics', (Springer, Dordrecht, Netherlands, 2006) pp. 249–273.
[23] J. M. Beckers, in 'ESO Conference on Very Large Telescopes and Their Instrumentation', Ed. By M. H. Ulrich, (European Southern Observatory, Garching, Germany, 1988), Vol. 2, pp. 693–703.
[24] B. L. Ellerbroek, J. Opt. Soc. Am. A 11, 783–805 (1994).
[25] L. Wang, A. Otarola, B, Ellerbroek, Proc. SPIE 7736-01 (2010).
[26] D. C. Senft, C. A. Hostetler, C. S. Gardner, Journal of Atmospheric and Terrestrial 55 (3), 425–439 (March 1993), ISSN 0021-9169, http://dx.doi.org/10.1016/0021-9169(93)90078-D. (http://www.sciencedirect.com/science/article/pii/002191699390078D).
[27] N. Moussaoui, B. R. Clemesha, R. Holzlöhner, D. M. Simonich, D. Bonaccini Calia, et al., A&A 511, A31 (2010).
[28] T. Pfrommer, P. Hickson, Proc. SPIE 8447 (2012); doi:10.1117/12.926056.
[29] Rigaut, F, Neichel, B, Monthly Notices of the Royal Astronomical Society: Letters 432 (1), 21–25 (2013).
[30] J. Alda, in 'Encyclopedia of Optical Engineering', (Marcel Dekker, New York, 2003) .
[31] L. C. Andrews and R. L. Philips, Laser Beam Propagation through Random Media, (SPIE Press, Bellingham, USA, 2005).
[32] R. Holzlöhner, D. Bonaccini Calia, W. Hackenberg, Proc. SPIE 7015, 701521–701521-11 (2008).
[33] D. T. Gavel, M. Ammons, B. Bauman, D. Dillon, E. Gates, et al., Proc. SPIE 7015-8 (2008).
[34] R. Holzlöhner, S. M. Rochester, D. Bonaccini Calia, D. Budker, J. M. Higbie, et al., Astron. & Astrophys. 510, A20 (2010).
[35] R. Holzlöhner, S. M. Rochester, T. Pfrommer, D. B. Calia, D. Budker, et al., Proc. SPIE 7736 (2010); doi:10.1117/12.856721; http://dx.doi.org/10.1117/12.856721.
[36] P. W. Milonni, R. Q. Fugate, J. M. Telle, J. Opt. Soc. Am. A 15, 217–233 (1998).
[37] E. Kibblewhite, Ch.4 in 'Laser Guide Star Adaptive Optics for Astronomy', Ed. By N. Ageorges, C. Dainty, (NATO ASI Series, Kluwer, 2000) pp. 67–87.
[38] Rochester Web. Internet location: http://budker.berkeley.edu/ADM/.
[39] R. Benumof, Am. J. Phys. 33, 151–160 (1965).
[40] D. Bonaccini Calia, I. Guidolin, A. Friedenauer, M. Hager, V. Karpov, et al., Proc. SPIE 8450-61 (2012).
[41] S. Olivier, D. Gavel, H. Friedman, C. Max, 44th Annual Meeting of the International Symposium on Optical Science, (Engineering, and Instrumentation Denver, Colorado, 1999).
[42] A. K. Hankla, J. Bartholomew, K. Groff, I. Lee, I. T. McKinnie, et al., Proc. SPIE 6782 (2006).
[43] C. d'Orgeville, S. Diggs, V. Fesquet, B. Neichel, W. Rambold et al., Proc. SPIE 8447 (2012).
[44] P. L. Wizinowich, D. Le Mignant, A. H. Bouchez, R. D. Campbell, J. C. Y. Chin, et al., Pub. Astron. Soc. Pacific, 118, 297–309 (2006).
[45] D. Bonaccini Calia, E. Allaert, J. L. Alvarez, C. Araujo Hauck, G. Avila, et al. Proc. SPIE 6272, (2006).
[46] D. Bonaccini Calia, Y. Feng, W. Hackenberg, R. Holzlöhner, L. Taylor, et al., The ESO Messenger 139, 12–19 (2010).
[47] S. A. E. Lewis, D. Bonaccini Calia, B. Buzzoni, P. Duhoux, G. Fischer, et al., Proc. AO4ELT3 (2013).
[48] A. Tracy, A. Hankla, C. Lopez, D. Sadighi, K. Grof, et al., Proc. SPIE 6100, 404–415 (2006).
[49] H. Takami, S. Colleya, M. Dinkinsa, M. Eldreda, O. Guyona, et al., Proc. SPIE Vol. 6272, 62720C (2006).
[50] J. E. Roberts, A. H. Bouchez, J. Angione, R. S. Burruss, J. L. Cromer, et al., Proc. SPIE 7015, (2008).
[51] C. A. Denman, J. D. Drummond, M. L. Eickhoff, R. Q. Fugate, P. D. Hillman, et al., Proc. SPIE 6272 (2006).
[52] S. Rabien, R. Davies, T. Ott, J. Li, R. Abuter, et al., SPIE 5490, 981 (2004).
[53] J. W. Dawson, Z. M. Liao, R. J. Beach, A. D. Drobshoff, S. A. Payne, et al., Patent US 7038844 B2 (2003).
[54] J. W. Dawson, A. D. Drobshoff, R. J. Beach, M. J. Messerly, S. A. Payne, et al., Proc. SPIE 6102 (2006).
[55] D. Bonaccini Calia, A. Friedenauer, V. Protopopov, I. Guidolin, L. R. Taylor, et al. SPIE Proc. 7736 (2010).
[56] R. Arsenault, P.-Y. Madec, J. Paufique, P. La Penna, S. Stroebele, et al., Proc. AO4ELT3 (2013), http://ao4elt3.sciencesconf.org/, id. # 118, article 118.
[57] Y. Feng, L. R. Taylor, D. Bonaccini Calia, Opt. Expr. 17, 19021–19026 (2009).
[58] R. Henselmans, D. Nijkerk, M. Lemmen, F. Kamphues, SPIE Integrated Modeling Symposium, Proc. SPIE 8447, (2012); doi:10.1117/12.926484.
[59] W. G. Kaenders, A. Friedenauer, V. Karpov, V. Protopopov, W. R. L. Clements, et al. Proc. SPIE 7736 (2010).
[60] H. T. Yura, Appl. Opt. 34, 2774 (1995).
[61] Y. E. Yenice, B. G. Evans, El. Lett. 35, 1875 (1999).
[62] L. Schreiber, T. Pfrommer, E. Diolaiti, SPIE, to appear (2014).
[63] D. Gratadour, G. Rousset, É. Gendron, O. Fauvarque, D. Bonaccini Calia, et al., Proc. SPIE 8447, Adaptive Optics Systems III, 84473N (September 13, 2012); doi: 10.1117/12.925720.
[64] D. Gavel, Proc. SPIE 8447 (2012).
[65] M. Lloyd-Hart, N. M. Milton, Proc. SPIE 4839 (2002).
[66] J. W. Beletic, S. Adkins, B. Burke, R. Reich, B. Kosicki, et al., Exp. Astron. 19, 103–109 (2005).
[67] G. Finger, I. Baker, D. Alvarez, Proc. SPIE 8453 (2012).
[68] P. Feautrier, Proceedings of the AO4ELT2 conference, (2013). http://ao4elt2.lesia.obspm.fr/spip.php?article543.
[69] M. Nicolle, T. Fusco, G. Rousset, V. Michau, Opt. Lett. 29, 2743 (2004).